Journal of Computational and Applied Mathematics 358 (2019) 279–292

Contents lists available at ScienceDirect

Journal of Computational and Applied Mathematics

journal homepage: www.elsevier.com/locate/cam

Fourier method for identifying electromagnetic sources with multi-frequency far-field data

Xianchao Wang [a], Minghui Song [a,*], Yukun Guo [a], Hongjie Li [b], Hongyu Liu [b,*]

[a] Department of mathematics, Harbin Institute of Technology, Harbin, 150001, China
[b] Department of Mathematics, Hong Kong Baptist University, Kowloon, Hong Kong Special Administrative Region

ARTICLE INFO

Article history:
Received 26 January 2018
Received in revised form 4 July 2018

MSC:
35R30
35P25
78A46

Keywords:
Inverse source problem
Maxwell system
Fourier expansion
Multi-frequency
Far-field

ABSTRACT

We consider the inverse problem of determining an unknown vectorial source current distribution associated with the homogeneous Maxwell system. We propose a novel non-iterative reconstruction method for solving the aforementioned inverse problem from multi-frequency far-field measurements. The method is based on recovering the Fourier coefficients of the unknown source. A key ingredient of the method is to establish the relationship between the Fourier coefficients and the multi-frequency far-field data. Uniqueness and stability results are established for the proposed reconstruction method. Numerical experiments are presented to illustrate the effectiveness and efficiency of the method.

1. Introduction

The inverse source problem is concerned with the reconstruction of an unknown/inaccessible active source from the measurement of the radiating field induced by the source. The inverse source problem arises in many important applications including acoustic tomography [1–4], medical imaging [5–7] and detection of pollution for the environment [8]. In this paper, we are mainly concerned with the inverse source problem for wave propagation in the time-harmonic regime. In the last decades, many theoretical and numerical studies have been done in dealing with the inverse source problem for wave scattering. The uniqueness and stability results can be found in [9–11]. Several numerical reconstruction methods have also been proposed and developed in the literature. For a fixed frequency, we refer the reader to [5,12,13]. However, with only one single frequency, the inverse source problem lacks of stability and it leads to severe ill-posedness. In order to improve the resolution, multi-frequency measurements should be employed in the reconstruction [9,14,15].

The goal of this paper is to develop a novel numerical scheme for reconstructing an electric current source associated with the time-harmonic Maxwell system. Due to the existence of non-radiating sources [16,17], the vectorial current sources cannot be uniquely determined from surface measurements. Albanese and Monk [18] showed that surface currents and dipole sources have a unique solution, but it is not valid for volume currents. Valdivia [15] showed that the volume currents could be uniquely identified if the current density is divergence free. Following the spirit of our earlier work [19–21] by three of the authors of using Fourier method for inverse acoustic source problem, we develop a Fourier method for the reconstruction of a volume current associated with the time-harmonic Maxwell system. The extension from the scalar

* Corresponding authors.
E-mail addresses: xcwang90@gmail.com (X. Wang), songmh@hit.edu.cn (M. Song), ykguo@hit.edu.cn (Y. Guo), hongjie_li@yeah.net (H. Li), hongyuliu@hkbu.edu.hk (H. Liu).

https://doi.org/10.1016/j.cam.2019.03.013
0377-0427/

Helmholtz equation to the vectorial Maxwell system involves much subtle and technical analysis. First, we establish the one-to-one correspondence between the Fourier coefficients and the far-field data, so that the Fourier coefficients can be directly calculated. Second, the proposed method is stable and robust to measurement noise. This is rigorously verified by establishing the corresponding stability estimates. Finally, compared to near-field Fourier method, our method is easy to implement with cheaper computational costs.

The rest of the paper is organized as follows. Section 2 describes the mathematical setup of the inverse source problem of our study. The theoretical uniqueness and stability results of proposed Fourier method are given in Sections 3 and 4, respectively. Section 5 presents several numerical examples to illustrate the effectiveness and efficiency of the proposed method.

2. Problem formulation

Consider the following time-harmonic Maxwell system in $\mathbb{R}^3$,

$$\begin{cases} \nabla \times \boldsymbol{E} - \mathrm{i}\omega\mu_0 \boldsymbol{H} = \boldsymbol{0}, \\ \nabla \times \boldsymbol{H} + \mathrm{i}\omega\varepsilon_0 \boldsymbol{E} = \boldsymbol{J}, \end{cases} \tag{2.1}$$

with the Silver–Müller radiation condition

$$\lim_{|\boldsymbol{x}|\to+\infty} |\boldsymbol{x}| \left(\sqrt{\mu_0}\boldsymbol{H} \times \hat{\boldsymbol{x}} - \sqrt{\varepsilon_0}\boldsymbol{E}\right) = \boldsymbol{0},$$

where $\hat{\boldsymbol{x}} = \boldsymbol{x}/|\boldsymbol{x}|$ and $\boldsymbol{x} = (x_1, x_2, x_3)^\top \in \mathbb{R}^3$. Throughout the rest of the paper, we use non-bold and bold fonts to signify scalar and vectorial quantities, respectively. In (2.1), $\boldsymbol{E}$ denotes the electric field, $\boldsymbol{H}$ denotes the magnetic field, $\boldsymbol{J}$ is an electric current density, ω denotes the frequency, ε_0 denotes the electric permittivity and μ_0 denotes the magnetic permeability of the isotropic homogeneous background medium. By eliminating $\boldsymbol{H}$ or $\boldsymbol{E}$ in (2.1), we obtain

$$\nabla \times \nabla \times \boldsymbol{E} - k^2 \boldsymbol{E} = \mathrm{i}\omega\mu_0 \boldsymbol{J},$$

and

$$\nabla \times \nabla \times \boldsymbol{H} - k^2 \boldsymbol{H} = \nabla \times \boldsymbol{J},$$

where $k := \omega\sqrt{\mu_0\varepsilon_0}$. With the help of the vectorial Green function [22], the radiated field can be written as

$$\boldsymbol{E}(\boldsymbol{x}) = \mathrm{i}\omega\mu_0 \left(\boldsymbol{I} + \frac{1}{k^2}\nabla\nabla\cdot\right) \int_{\mathbb{R}^3} \Phi(\boldsymbol{x}, \boldsymbol{y}) \boldsymbol{J}(\boldsymbol{y})\, \mathrm{d}\boldsymbol{y}, \tag{2.2}$$

and

$$\boldsymbol{H}(\boldsymbol{x}) = \nabla \times \int_{\mathbb{R}^3} \Phi(\boldsymbol{x}, \boldsymbol{y}) \boldsymbol{J}(\boldsymbol{y})\, \mathrm{d}\boldsymbol{y}, \tag{2.3}$$

respectively, where $\boldsymbol{I}$ is the 3×3 identity matrix and

$$\Phi(\boldsymbol{x}, \boldsymbol{y}) = \frac{\mathrm{e}^{\mathrm{i}k|\boldsymbol{x}-\boldsymbol{y}|}}{4\pi|\boldsymbol{x}-\boldsymbol{y}|}, \quad \boldsymbol{x} \neq \boldsymbol{y},$$

is the fundamental solution to the Helmholtz equation. The radiating fields $\boldsymbol{E}, \boldsymbol{H}$ to the Maxwell system have the following asymptotic expansion [23]

$$\boldsymbol{E}(\boldsymbol{x}) = \frac{e^{\mathrm{i}k|\boldsymbol{x}|}}{|\boldsymbol{x}|} \left\{ \boldsymbol{E}_\infty(\hat{\boldsymbol{x}}) + \mathcal{O}\left(\frac{1}{|\boldsymbol{x}|}\right) \right\}, \quad |\boldsymbol{x}| \to +\infty,$$

$$\boldsymbol{H}(\boldsymbol{x}) = \frac{e^{\mathrm{i}k|\boldsymbol{x}|}}{|\boldsymbol{x}|} \left\{ \boldsymbol{H}_\infty(\hat{\boldsymbol{x}}) + \mathcal{O}\left(\frac{1}{|\boldsymbol{x}|}\right) \right\}, \quad |\boldsymbol{x}| \to +\infty,$$

and by using the integral representations (2.2) and (2.3), we have

$$\boldsymbol{E}_\infty(\hat{\boldsymbol{x}}) = \frac{\mathrm{i}\omega\mu_0}{4\pi} \left(\boldsymbol{I} - \hat{\boldsymbol{x}}\hat{\boldsymbol{x}}^\top\right) \int_{\mathbb{R}^3} e^{-\mathrm{i}k\hat{\boldsymbol{x}}\cdot\boldsymbol{y}} \boldsymbol{J}(\boldsymbol{y})\, \mathrm{d}\boldsymbol{y}, \tag{2.4}$$

$$\boldsymbol{H}_\infty(\hat{\boldsymbol{x}}) = \frac{\mathrm{i}k}{4\pi} \hat{\boldsymbol{x}} \times \int_{\mathbb{R}^3} e^{-\mathrm{i}k\hat{\boldsymbol{x}}\cdot\boldsymbol{y}} \boldsymbol{J}(\boldsymbol{y})\, \mathrm{d}\boldsymbol{y}. \tag{2.5}$$

Let $\boldsymbol{\nu}$ be the unit outward normal of the unit sphere $\mathbb{S}^2$. Define the space of surface tangential vector fields in $L^2(\mathbb{S}^2)$ by

$$L_t^2(\mathbb{S}^2) := \left\{ \boldsymbol{h} \in \left(L^2(\mathbb{S}^2)\right)^3 \mid \boldsymbol{h} \cdot \boldsymbol{\nu} = 0 \ \text{ on } \ \mathbb{S}^2 \right\},$$

then the electric far field pattern and magnetic far field pattern satisfy $E_\infty(\hat{\boldsymbol{x}}) \in L_t^2(\mathbb{S}^2)$ and $H_\infty(\hat{\boldsymbol{x}}) \in L_t^2(\mathbb{S}^2)$, respectively.

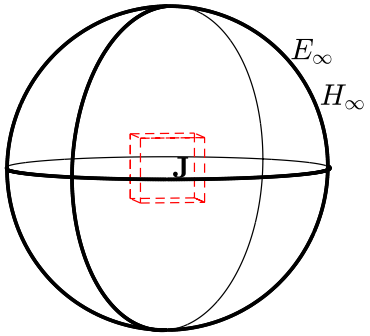

Fig. 1. The schematic illustration of the inverse electromagnetic source problem by the far-field measurements.

In what follows, we always assume that the electromagnetic source is a volume current that is supported in D. As mentioned earlier, there exist non-radiating sources that produce no radiating field outside D. Hence, without any a prior knowledge, one can only recover the radiating part of the current density distribution. In order to formulate the uniqueness result, we assume that the current density distribution $\boldsymbol{J}$ only consists of radiating source, which is independent of the wavenumber k and of the form

$$\boldsymbol{J} \in \left(L^2(\mathbb{R}^3)\right)^3, \quad \operatorname{supp} \boldsymbol{J} \subset D,$$

where D is a cube. Furthermore, the current density distribution $\boldsymbol{J}$ satisfies the transverse electric (TE) and transverse magnetic (TM) decomposition; that is, the source can be expressed in the form

$$\boldsymbol{J} = \boldsymbol{p}f + \boldsymbol{p} \times \nabla g, \tag{2.6}$$

where $f \in L^2(D)$ and $g \in H^1(D)$. We also refer to [24] for more details on the TE/TM decomposition. Here, $\boldsymbol{p}$ is the polarization direction which is assumed to be known and yields the following admissible set

$$\mathbb{P} := \left\{\boldsymbol{p} \in \mathbb{S}^2 \mid \boldsymbol{p} \times \boldsymbol{l} \neq \boldsymbol{0}, \quad \boldsymbol{l} \in \mathbb{Z}^3 \backslash \{\boldsymbol{0}\}\right\}. \tag{2.7}$$

Fig. 1 provides a schematic illustration of the geometric setting of the measurements. With the above discussion, the inverse source problem of the current study can be stated as follows:

Inverse Problem. Given a fixed polarization direction $\boldsymbol{p} \in \mathbb{P}$ and a finite number of wavenumbers $\{k\}$, we intend to recover the electromagnetic source $\boldsymbol{J}$ defined in (2.6) from the electric far-field data $\{\boldsymbol{E}_\infty(\hat{\boldsymbol{x}}_k; k, \boldsymbol{p})\}$ or the magnetic far-field data $\{\boldsymbol{H}_\infty(\hat{\boldsymbol{x}}_k; k, \boldsymbol{p})\}$, where $\hat{\boldsymbol{x}}_k \in \mathbb{S}^2$ depends on the wavenumber k.

3. Uniqueness

Prior to our discussion, we introduce some notations and relevant Sobolev spaces. Without loss of generality, we let

$$D = \left(-\frac{a}{2}, \frac{a}{2}\right)^3, \quad a \in \mathbb{R}_+.$$

Introduce the Fourier basis functions that are defined by

$$\phi_{\boldsymbol{l}}(\boldsymbol{x}) = \exp\left(\mathrm{i}\frac{2\pi}{a}\boldsymbol{l} \cdot \boldsymbol{x}\right), \quad \boldsymbol{l} \in \mathbb{Z}^3, \ \boldsymbol{x} \in \mathbb{R}^3. \tag{3.1}$$

By using the Fourier series expansion, the scalar functions $f \in L^2(D)$ and $g \in H^1(D)$ can be written as

$$f = \sum_{\boldsymbol{l} \in \mathbb{Z}^3} \hat{f}_{\boldsymbol{l}}\, \phi_{\boldsymbol{l}}, \quad g = \sum_{\boldsymbol{l} \in \mathbb{Z}^3 \backslash \{\boldsymbol{0}\}} \hat{g}_{\boldsymbol{l}}\, \phi_{\boldsymbol{l}},$$

where the Fourier coefficients are given by

$$\hat{f}_{\boldsymbol{l}} = \frac{1}{a^3} \int_D f(\boldsymbol{x}) \overline{\phi_{\boldsymbol{l}}(\boldsymbol{x})}\, \mathrm{d}\boldsymbol{x}, \tag{3.2}$$

$$\hat{g}_{\boldsymbol{l}} = \frac{1}{a^3} \int_D g(\boldsymbol{x}) \overline{\phi_{\boldsymbol{l}}(\boldsymbol{x})}\, \mathrm{d}\boldsymbol{x}, \tag{3.3}$$

where the overbar stands for the complex conjugate in this paper. Therefore the Fourier expansion of the current density $\boldsymbol{J}$ is

$$\boldsymbol{J} = \boldsymbol{p}f + \boldsymbol{p} \times \nabla g = \boldsymbol{p} \sum_{\boldsymbol{l} \in \mathbb{Z}^3} \hat{f}_{\boldsymbol{l}}\, \phi_{\boldsymbol{l}} + \frac{2\pi \mathrm{i}}{a} \sum_{\boldsymbol{l} \in \mathbb{Z}^3 \setminus \{\boldsymbol{0}\}} (\boldsymbol{p} \times \boldsymbol{l})\, \hat{g}_{\boldsymbol{l}}\, \phi_{\boldsymbol{l}}. \tag{3.4}$$

The proposed reconstruction scheme in the current article is based on determining the Fourier coefficients $\hat{f}_{\boldsymbol{l}}$ and $\hat{g}_{\boldsymbol{l}}$ of the current density by using the corresponding electric or magnetic far-field data. For the subsequent use, we introduce the Sobolev spaces with $\sigma > 0$

$$(H_{\boldsymbol{p}}^{\sigma}(D))^3 := \left\{ \boldsymbol{p}f + \boldsymbol{p} \times \nabla g \mid f \in H^{\sigma}(D),\ g \in H^{\sigma+1}(D),\ \boldsymbol{p} \in \mathbb{S}^2 \right\},$$

equipped with the norm

$$\|\boldsymbol{G}\|_{\boldsymbol{p},\sigma} = \left(\sum_{\boldsymbol{l} \in \mathbb{Z}^3} \left(1 + |\boldsymbol{l}|^2\right)^{\sigma} |\hat{f}_{\boldsymbol{l}}|^2 + \frac{4\pi^2}{a^2} \sum_{\boldsymbol{l} \in \mathbb{Z}^3 \setminus \{\boldsymbol{0}\}} \left(1 + |\boldsymbol{l}|^2\right)^{\sigma} |\boldsymbol{p} \times \boldsymbol{l}|^2 |\hat{g}_{\boldsymbol{l}}|^2 \right)^{1/2},$$

where $\boldsymbol{G} \in (H_{\boldsymbol{p}}^{\sigma}(D))^3$ has the Fourier expansion of the form

$$\boldsymbol{G} = \boldsymbol{p} \sum_{\boldsymbol{l} \in \mathbb{Z}^3} \hat{f}_{\boldsymbol{l}}\, \phi_{\boldsymbol{l}} + \frac{2\pi \mathrm{i}}{a} \sum_{\boldsymbol{l} \in \mathbb{Z}^3 \setminus \{\boldsymbol{0}\}} (\boldsymbol{p} \times \boldsymbol{l})\, \hat{g}_{\boldsymbol{l}}\, \phi_{\boldsymbol{l}}.$$

In addition, the wavenumber cannot be zero in (2.4) and (2.5). Following [20], we introduce the following definition of wavenumbers.

Definition 3.1 (*Admissible Wavenumbers*)**.** Let λ be a sufficiently small positive constant and the admissible wavenumbers can be defined by

$$k_{\boldsymbol{l}} := \begin{cases} \dfrac{2\pi}{a} |\boldsymbol{l}|, & \boldsymbol{l} \in \mathbb{Z}^3 \setminus \{\boldsymbol{0}\}, \\ \dfrac{2\pi}{a} \lambda, & \boldsymbol{l} = \boldsymbol{0}. \end{cases} \tag{3.5}$$

Correspondingly, the observation direction is given by

$$\hat{\boldsymbol{x}}_{\boldsymbol{l}} := \begin{cases} \dfrac{\boldsymbol{l}}{|\boldsymbol{l}|}, & \boldsymbol{l} \in \mathbb{Z}^3 \setminus \{\boldsymbol{0}\}, \\ (1, 0, 0), & \boldsymbol{l} = \boldsymbol{0}. \end{cases} \tag{3.6}$$

By virtue of Definition 3.1, the Fourier basis functions defined in (3.1) could be written as

$$\phi_{\boldsymbol{l}}(\boldsymbol{x}) = \exp\left(\mathrm{i} k_{\boldsymbol{l}}\, \hat{\boldsymbol{l}} \cdot \boldsymbol{x}\right), \quad \boldsymbol{l} \in \mathbb{Z}^3,\ \boldsymbol{x} \in \mathbb{R}^3.$$

Next we state the uniqueness result.

Theorem 3.1. *Let $k_{\boldsymbol{l}}$ and $\hat{\boldsymbol{x}}_{\boldsymbol{l}}$ be defined in (3.5) and (3.6), then the Fourier coefficients $\{\hat{f}_{\boldsymbol{l}}\}$ and $\{\hat{g}_{\boldsymbol{l}}\}$ in (3.2) and (3.3) could be uniquely determined by $\{\boldsymbol{E}_{\infty}(\hat{\boldsymbol{x}}_{\boldsymbol{l}}; k_{\boldsymbol{l}}, \boldsymbol{p})\}$ or $\{\boldsymbol{H}_{\infty}(\hat{\boldsymbol{x}}_{\boldsymbol{l}}; k_{\boldsymbol{l}}, \boldsymbol{p})\}$, where $\boldsymbol{l} \in \mathbb{Z}^3$ and $\boldsymbol{p} \in \mathbb{P}$ is a fixed polarization direction.*

Proof. For simplicity, we write $\boldsymbol{E}_{\infty}(\hat{\boldsymbol{x}}_{\boldsymbol{l}}; k_{\boldsymbol{l}})$ and $\boldsymbol{H}_{\infty}(\hat{\boldsymbol{x}}_{\boldsymbol{l}}; k_{\boldsymbol{l}})$ for $\boldsymbol{E}_{\infty}(\hat{\boldsymbol{x}}_{\boldsymbol{l}}; k_{\boldsymbol{l}}, \boldsymbol{p})$ and $\boldsymbol{H}_{\infty}(\hat{\boldsymbol{x}}_{\boldsymbol{l}}; k_{\boldsymbol{l}}, \boldsymbol{p})$ with a fixed polarization direction $\boldsymbol{p} \in \mathbb{P}$. Let $\boldsymbol{J}$ be the electromagnetic source that produces the electric far-field data $\{\boldsymbol{E}_{\infty}(\hat{\boldsymbol{x}}_{\boldsymbol{l}}; k_{\boldsymbol{l}})\}_{\boldsymbol{l} \in \mathbb{Z}^3}$ and the magnetic far-field data $\{\boldsymbol{H}_{\infty}(\hat{\boldsymbol{x}}_{\boldsymbol{l}}; k_{\boldsymbol{l}})\}_{\boldsymbol{l} \in \mathbb{Z}^3}$ on $\mathbb{S}^2$.

First, we consider the recovery of $\boldsymbol{J}$ by the magnetic far-field data. For every $\boldsymbol{l} \in \mathbb{Z}^3 \setminus \{\boldsymbol{0}\}$, using (2.5) and (3.4), we have

$$\begin{aligned} &\boldsymbol{H}_{\infty}(\hat{\boldsymbol{x}}_{\boldsymbol{l}}; k_{\boldsymbol{l}}) \\ &= \frac{\mathrm{i} k_{\boldsymbol{l}}}{4\pi} \hat{\boldsymbol{x}}_{\boldsymbol{l}} \times \int_D \left(\boldsymbol{p} \hat{f}_{\boldsymbol{0}} \mathrm{e}^{-\mathrm{i} k_{\boldsymbol{l}} \hat{\boldsymbol{x}}_{\boldsymbol{l}} \cdot \boldsymbol{y}} + \sum_{\tilde{\boldsymbol{l}} \in \mathbb{Z}^3 \setminus \{\boldsymbol{0}\}} \left(\boldsymbol{p} \hat{f}_{\tilde{\boldsymbol{l}}} + \frac{2\pi \mathrm{i}}{a} (\boldsymbol{p} \times \tilde{\boldsymbol{l}}) \hat{g}_{\tilde{\boldsymbol{l}}} \right) \mathrm{e}^{\mathrm{i}(k_{\tilde{\boldsymbol{l}}} \hat{\tilde{\boldsymbol{l}}} - k_{\boldsymbol{l}} \hat{\boldsymbol{x}}_{\boldsymbol{l}}) \cdot \boldsymbol{y}} \right) \mathrm{d}\boldsymbol{y} \\ &= \frac{\mathrm{i} k_{\boldsymbol{l}} a^3}{4\pi} \left(\hat{\boldsymbol{x}}_{\boldsymbol{l}} \times \boldsymbol{p} \hat{f}_{\boldsymbol{l}} + \frac{2\pi \mathrm{i}}{a} \hat{\boldsymbol{x}}_{\boldsymbol{l}} \times (\boldsymbol{p} \times \boldsymbol{l}) \hat{g}_{\boldsymbol{l}} \right). \end{aligned} \tag{3.7}$$

From (2.7) and (3.6), we see that $\{\hat{\boldsymbol{x}}_{\boldsymbol{l}}, \boldsymbol{p} \times \hat{\boldsymbol{x}}_{\boldsymbol{l}}, \hat{\boldsymbol{x}}_{\boldsymbol{l}} \times (\boldsymbol{p} \times \hat{\boldsymbol{x}}_{\boldsymbol{l}})\}$ forms an orthogonal basis of $\mathbb{R}^3$. Multiplying $\hat{\boldsymbol{x}}_{\boldsymbol{l}} \times \boldsymbol{p}$ on the both sides of (3.7), and using the orthogonality, we obtain

$$\hat{f}_{\boldsymbol{l}} = \frac{4\pi\, \hat{\boldsymbol{x}}_{\boldsymbol{l}} \times \boldsymbol{p} \cdot \boldsymbol{H}_{\infty}(\hat{\boldsymbol{x}}_{\boldsymbol{l}}; k_{\boldsymbol{l}})}{\mathrm{i} k_{\boldsymbol{l}} a^3 |\hat{\boldsymbol{x}}_{\boldsymbol{l}} \times \boldsymbol{p}|^2}, \tag{3.8}$$

where $|\cdot|$ denotes the ℓ^2 norm. Similarly, multiplying $\hat{\boldsymbol{x}}_{\boldsymbol{l}} \times (\boldsymbol{p} \times \boldsymbol{l})$ on the both sides of (3.7), we have

$$\hat{g}_{\boldsymbol{l}} = -\frac{2\hat{\boldsymbol{x}}_{\boldsymbol{l}} \times (\boldsymbol{p} \times \boldsymbol{l}) \cdot \boldsymbol{H}_\infty(\hat{\boldsymbol{x}}_{\boldsymbol{l}}; k_{\boldsymbol{l}})}{k_{\boldsymbol{l}} a^2 |\hat{\boldsymbol{x}}_{\boldsymbol{l}} \times (\boldsymbol{p} \times \boldsymbol{l})|^2}. \tag{3.9}$$

For $\boldsymbol{l} = \boldsymbol{0}$, we have

$$\begin{aligned}
&\boldsymbol{H}_\infty(\hat{\boldsymbol{x}}_{\boldsymbol{0}}; k_{\boldsymbol{0}}) \\
&= \frac{\mathrm{i}k_{\boldsymbol{0}}}{4\pi} \hat{\boldsymbol{x}}_{\boldsymbol{0}} \times \int_D \left(\boldsymbol{p}\hat{f}_{\boldsymbol{0}} \mathrm{e}^{-\mathrm{i}k_{\boldsymbol{0}}\hat{\boldsymbol{x}}_{\boldsymbol{0}} \cdot \boldsymbol{y}} + \sum_{\boldsymbol{l} \in \mathbb{Z}^3 \setminus \{\boldsymbol{0}\}} \left(\boldsymbol{p}\hat{f}_{\boldsymbol{l}} + \frac{2\pi \mathrm{i}}{a} (\boldsymbol{p} \times \boldsymbol{l}) \hat{g}_{\boldsymbol{l}} \right) \mathrm{e}^{\mathrm{i}(k_{\boldsymbol{l}}\hat{\boldsymbol{l}} - k_{\boldsymbol{0}}\hat{\boldsymbol{x}}_{\boldsymbol{0}}) \cdot \boldsymbol{y}} \right) \mathrm{d}\boldsymbol{y}.
\end{aligned}$$

Multiplying $\hat{\boldsymbol{x}}_{\boldsymbol{0}} \times \boldsymbol{p}$ on the both sides of the last equation, and also using the orthogonality, we obtain

$$\hat{\boldsymbol{x}}_{\boldsymbol{0}} \times \boldsymbol{p} \cdot \boldsymbol{H}_\infty(\hat{\boldsymbol{x}}_{\boldsymbol{0}}; k_{\boldsymbol{0}}) = \frac{\mathrm{i}k_{\boldsymbol{0}}}{4\pi} |\hat{\boldsymbol{x}}_{\boldsymbol{0}} \times \boldsymbol{p}|^2 \left(a^3 \hat{f}_{\boldsymbol{0}} \frac{\sin \lambda\pi}{\lambda\pi} + \sum_{\boldsymbol{l} \in \mathbb{Z}^3 \setminus \{\boldsymbol{0}\}} \hat{f}_{\boldsymbol{l}} \int_D \mathrm{e}^{\mathrm{i}(k_{\boldsymbol{l}}\hat{\boldsymbol{l}} - k_{\boldsymbol{0}}\hat{\boldsymbol{x}}_{\boldsymbol{0}}) \cdot \boldsymbol{y}} \, \mathrm{d}\boldsymbol{y} \right).$$

Thus,

$$\hat{f}_{\boldsymbol{0}} = \frac{\lambda\pi}{a^3 \sin \lambda\pi} \left(\frac{4\pi \hat{\boldsymbol{x}}_{\boldsymbol{0}} \times \boldsymbol{p} \cdot \boldsymbol{H}_\infty(\hat{\boldsymbol{x}}_{\boldsymbol{0}}; k_{\boldsymbol{0}})}{\mathrm{i}k_{\boldsymbol{0}} |\hat{\boldsymbol{x}}_{\boldsymbol{0}} \times \boldsymbol{p}|^2} - \sum_{\boldsymbol{l} \in \mathbb{Z}^3 \setminus \{\boldsymbol{0}\}} \hat{f}_{\boldsymbol{l}} \int_D \mathrm{e}^{\mathrm{i}(k_{\boldsymbol{l}}\hat{\boldsymbol{l}} - k_{\boldsymbol{0}}\hat{\boldsymbol{x}}_{\boldsymbol{0}}) \cdot \boldsymbol{y}} \, \mathrm{d}\boldsymbol{y} \right). \tag{3.10}$$

Next, we consider the recovery of $\boldsymbol{J}$ by the electric far-field data. For every $\boldsymbol{l} \in \mathbb{Z}^3 \setminus \{\boldsymbol{0}\}$, using (2.4) and (3.4), we have

$$\boldsymbol{E}_\infty(\hat{\boldsymbol{x}}_{\boldsymbol{l}}; k_{\boldsymbol{l}}) = \frac{\mathrm{i}\omega\mu_0 a^3}{4\pi} \left(\boldsymbol{I} - \hat{\boldsymbol{x}}_{\boldsymbol{l}} \hat{\boldsymbol{x}}_{\boldsymbol{l}}^\top \right) \left(\boldsymbol{p}\hat{f}_{\boldsymbol{l}} + \frac{2\pi \mathrm{i}}{a} (\boldsymbol{p} \times \boldsymbol{l}) \hat{g}_{\boldsymbol{l}} \right). \tag{3.11}$$

Through straightforward calculations, one can verify that

$$\hat{\boldsymbol{x}}_{\boldsymbol{l}} \times (\hat{\boldsymbol{x}}_{\boldsymbol{l}} \times \boldsymbol{A}) = -\left(\boldsymbol{I} - \hat{\boldsymbol{x}}_{\boldsymbol{l}} \hat{\boldsymbol{x}}_{\boldsymbol{l}}^\top \right) \boldsymbol{A}, \quad \forall \boldsymbol{A} \in \mathbb{R}^3.$$

Combining the last two equations, one can show that

$$\boldsymbol{E}_\infty(\hat{\boldsymbol{x}}_{\boldsymbol{l}}; k_{\boldsymbol{l}}) = \frac{\mathrm{i}\omega\mu_0 a^3}{4\pi} \left(-\hat{\boldsymbol{x}}_{\boldsymbol{l}} \times (\hat{\boldsymbol{x}}_{\boldsymbol{l}} \times \boldsymbol{p}) \hat{f}_{\boldsymbol{l}} - \frac{2\pi \mathrm{i}}{a} \hat{\boldsymbol{x}}_{\boldsymbol{l}} \times (\hat{\boldsymbol{x}}_{\boldsymbol{l}} \times (\boldsymbol{p} \times \boldsymbol{l})) \hat{g}_{\boldsymbol{l}} \right). \tag{3.12}$$

Multiplying $\boldsymbol{p}$ on the both sides of (3.12), and using the orthogonality, we obtain

$$\begin{aligned}
&\boldsymbol{p} \cdot \boldsymbol{E}_\infty(\hat{\boldsymbol{x}}_{\boldsymbol{l}}; k_{\boldsymbol{l}}) \\
&= \frac{\mathrm{i}\omega\mu_0 a^3}{4\pi} \left(-\boldsymbol{p} \cdot \hat{\boldsymbol{x}}_{\boldsymbol{l}} \times (\hat{\boldsymbol{x}}_{\boldsymbol{l}} \times \boldsymbol{p}) \hat{f}_{\boldsymbol{l}} - \frac{2\pi \mathrm{i}}{a} \boldsymbol{p} \cdot \hat{\boldsymbol{x}}_{\boldsymbol{l}} \times (\hat{\boldsymbol{x}}_{\boldsymbol{l}} \times (\boldsymbol{p} \times \boldsymbol{l})) \hat{g}_{\boldsymbol{l}} \right) \\
&= \frac{\mathrm{i}\omega\mu_0 a^3}{4\pi} \left((\hat{\boldsymbol{x}}_{\boldsymbol{l}} \times \boldsymbol{p}) \cdot (\hat{\boldsymbol{x}}_{\boldsymbol{l}} \times \boldsymbol{p}) \hat{f}_{\boldsymbol{l}} + \frac{2\pi \mathrm{i}}{a} (\hat{\boldsymbol{x}}_{\boldsymbol{l}} \times \boldsymbol{p}) \cdot (\hat{\boldsymbol{x}}_{\boldsymbol{l}} \times (\boldsymbol{p} \times \boldsymbol{l})) \hat{g}_{\boldsymbol{l}} \right) \\
&= \frac{\mathrm{i}\omega\mu_0 a^3}{4\pi} \left| \hat{\boldsymbol{x}}_{\boldsymbol{l}} \times \boldsymbol{p} \right|^2 \hat{f}_{\boldsymbol{l}}.
\end{aligned}$$

Thus,

$$\hat{f}_{\boldsymbol{l}} = \frac{4\pi \boldsymbol{p} \cdot \boldsymbol{E}_\infty(\hat{\boldsymbol{x}}_{\boldsymbol{l}}; k_{\boldsymbol{l}})}{\mathrm{i}\omega\mu_0 a^3 |\hat{\boldsymbol{x}}_{\boldsymbol{l}} \times \boldsymbol{p}|^2}. \tag{3.13}$$

Similarly, multiplying $\boldsymbol{p} \times \boldsymbol{l}$ on the both sides of (3.12), we obtain

$$\hat{g}_{\boldsymbol{l}} = -\frac{2(\boldsymbol{p} \times \boldsymbol{l}) \cdot \boldsymbol{E}_\infty(\hat{\boldsymbol{x}}_{\boldsymbol{l}}; k_{\boldsymbol{l}})}{\omega\mu_0 a^2 |\hat{\boldsymbol{x}}_{\boldsymbol{l}} \times (\boldsymbol{p} \times \boldsymbol{l})|^2}. \tag{3.14}$$

For $\boldsymbol{l} = \boldsymbol{0}$, we have

$$\begin{aligned}
&\boldsymbol{E}_\infty(\hat{\boldsymbol{x}}_{\boldsymbol{0}}; k_{\boldsymbol{0}}) \\
&= \frac{\mathrm{i}\omega\mu_0}{4\pi} \left(\boldsymbol{I} - \hat{\boldsymbol{x}}_{\boldsymbol{0}} \hat{\boldsymbol{x}}_{\boldsymbol{0}}^\top \right) \int_D \left(\boldsymbol{p}\hat{f}_{\boldsymbol{0}} \mathrm{e}^{-\mathrm{i}k_{\boldsymbol{0}}\hat{\boldsymbol{x}}_{\boldsymbol{0}} \cdot \boldsymbol{y}} + \sum_{\boldsymbol{l} \in \mathbb{Z}^3 \setminus \{\boldsymbol{0}\}} \left(\boldsymbol{p}\hat{f}_{\boldsymbol{l}} + \frac{2\pi \mathrm{i}}{a} (\boldsymbol{p} \times \boldsymbol{l}) \hat{g}_{\boldsymbol{l}} \right) \mathrm{e}^{\mathrm{i}(k_{\boldsymbol{l}}\hat{\boldsymbol{l}} - k_{\boldsymbol{0}}\hat{\boldsymbol{x}}_{\boldsymbol{0}}) \cdot \boldsymbol{y}} \right) \mathrm{d}\boldsymbol{y}.
\end{aligned}$$

Multiplying $\boldsymbol{p}$ on the both sides of the last equation, and also using the orthogonality, we obtain

$$\boldsymbol{p} \cdot \boldsymbol{E}_\infty(\hat{\boldsymbol{x}}_{\boldsymbol{0}}; k_{\boldsymbol{0}}) = \frac{\mathrm{i}\omega\mu_0}{4\pi} |\hat{\boldsymbol{x}}_{\boldsymbol{0}} \times \boldsymbol{p}|^2 \left(a^3 \hat{f}_{\boldsymbol{0}} \frac{\sin \lambda\pi}{\lambda\pi} + \sum_{\boldsymbol{l} \in \mathbb{Z}^3 \setminus \{\boldsymbol{0}\}} \hat{f}_{\boldsymbol{l}} \int_D \mathrm{e}^{\mathrm{i}(k_{\boldsymbol{l}}\hat{\boldsymbol{l}} - k_{\boldsymbol{0}}\hat{\boldsymbol{x}}_{\boldsymbol{0}}) \cdot \boldsymbol{y}} \, \mathrm{d}\boldsymbol{y} \right).$$

Thus,

$$\hat{f}_{\mathbf{0}} = \frac{\lambda\pi}{a^3 \sin\lambda\pi}\left(\frac{4\pi \boldsymbol{p}\cdot \boldsymbol{E}_\infty(\hat{\boldsymbol{x}}_{\mathbf{0}};k_{\mathbf{0}})}{\mathrm{i}\omega\mu_0|\hat{\boldsymbol{x}}_{\mathbf{0}}\times\boldsymbol{p}|^2} - \sum_{\boldsymbol{l}\in\mathbb{Z}^3\setminus\{\mathbf{0}\}} \hat{f}_{\boldsymbol{l}} \int_D \mathrm{e}^{\mathrm{i}(k_{\boldsymbol{l}}\hat{\boldsymbol{l}}-k_{\mathbf{0}}\hat{\boldsymbol{x}}_{\mathbf{0}})\cdot\boldsymbol{y}}\,\mathrm{d}\boldsymbol{y}\right).$$

The proof is complete. □

In practical computations, we have to truncate the infinite series by a finite order $N \in \mathbb{N}$ to approximate $\boldsymbol{J}$ by

$$\boldsymbol{J}_N = \boldsymbol{p}\hat{f}_{\mathbf{0}} + \sum_{1\le|\boldsymbol{l}|_\infty\le N}\left(\boldsymbol{p}\hat{f}_{\boldsymbol{l}} + \frac{2\pi\mathrm{i}}{a}(\boldsymbol{p}\times\boldsymbol{l})\hat{g}_{\boldsymbol{l}}\right)\phi_{\boldsymbol{l}}, \tag{3.15}$$

where $\hat{f}_{\mathbf{0}}$ could be represented by magnetic far-field

$$\hat{f}_{\mathbf{0}} \approx \frac{\lambda\pi}{a^3 \sin\lambda\pi}\left(\frac{4\pi \hat{\boldsymbol{x}}_{\mathbf{0}}\times\boldsymbol{p}\cdot \boldsymbol{H}_\infty(\hat{\boldsymbol{x}}_{\mathbf{0}};k_{\mathbf{0}})}{\mathrm{i}k_{\mathbf{0}}|\hat{\boldsymbol{x}}_{\mathbf{0}}\times\boldsymbol{p}|^2} - \sum_{1\le|\boldsymbol{l}|_\infty\le N} \hat{f}_{\boldsymbol{l}} \int_D \mathrm{e}^{\mathrm{i}(k_{\boldsymbol{l}}\hat{\boldsymbol{l}}-k_{\mathbf{0}}\hat{\boldsymbol{x}}_{\mathbf{0}})\cdot\boldsymbol{y}}\,\mathrm{d}\boldsymbol{y}\right), \tag{3.16}$$

or electric far-field

$$\hat{f}_{\mathbf{0}} \approx \frac{\lambda\pi}{a^3 \sin\lambda\pi}\left(\frac{4\pi \boldsymbol{p}\cdot \boldsymbol{E}_\infty(\hat{\boldsymbol{x}}_{\mathbf{0}};k_{\mathbf{0}})}{\mathrm{i}\omega\mu_0|\hat{\boldsymbol{x}}_{\mathbf{0}}\times\boldsymbol{p}|^2} - \sum_{1\le|\boldsymbol{l}|_\infty\le N} \hat{f}_{\boldsymbol{l}} \int_D \mathrm{e}^{\mathrm{i}(k_{\boldsymbol{l}}\hat{\boldsymbol{l}}-k_{\mathbf{0}}\hat{\boldsymbol{x}}_{\mathbf{0}})\cdot\boldsymbol{y}}\,\mathrm{d}\boldsymbol{y}\right). \tag{3.17}$$

4. Stability

In this section, we derive the stability estimates of recovering the Fourier coefficients of the electric current source by using the far-field data. We only consider the stability of using the magnetic far-field data, and the case with the electric far-field data can be treated in a similar manner. In what follows, we introduce $\boldsymbol{H}^\delta_\infty(\hat{\boldsymbol{x}}_{\boldsymbol{l}};k_{\boldsymbol{l}})$ such that

$$|\boldsymbol{H}^\delta_\infty(\hat{\boldsymbol{x}}_{\boldsymbol{l}};k_{\boldsymbol{l}}) - \boldsymbol{H}_\infty(\hat{\boldsymbol{x}}_{\boldsymbol{l}};k_{\boldsymbol{l}})| \le \delta|\boldsymbol{H}_\infty(\hat{\boldsymbol{x}}_{\boldsymbol{l}};k_{\boldsymbol{l}})|,$$

where $|\cdot|$ denotes the ℓ^2 norm and $\delta > 0$. We first present two auxiliary results.

Theorem 4.1. *For $\boldsymbol{l}\in\mathbb{Z}^3$, $|\boldsymbol{l}|_\infty \le N$, we have*

$$|\hat{f}^\delta_{\boldsymbol{l}} - \hat{f}_{\boldsymbol{l}}| \le C_1\delta, \qquad 1\le|\boldsymbol{l}|_\infty\le N, \tag{4.1}$$

$$|\hat{g}^\delta_{\boldsymbol{l}} - \hat{g}_{\boldsymbol{l}}| \le C_2\delta, \qquad 1\le|\boldsymbol{l}|_\infty\le N, \tag{4.2}$$

$$|\hat{f}^\delta_{\mathbf{0}} - \hat{f}_{\mathbf{0}}| \le C_3\delta + C_4\lambda N\delta + C_5\frac{\lambda}{\sqrt{N}}, \tag{4.3}$$

where constants C_1, C_2, C_3, C_4 and C_5 depend on f, g, a and λ.

Proof. For $\boldsymbol{l}\in\mathbb{Z}^3\setminus\{\mathbf{0}\}$, from Schwarz inequality and (3.8), we have

$$\begin{aligned}
|\hat{f}^\delta_{\boldsymbol{l}} - \hat{f}_{\boldsymbol{l}}| &= \left|\frac{4\pi\hat{\boldsymbol{x}}_{\boldsymbol{l}}\times\boldsymbol{p}}{\mathrm{i}k_{\boldsymbol{l}}a^3|\hat{\boldsymbol{x}}_{\boldsymbol{l}}\times\boldsymbol{p}|^2}\cdot\left(\boldsymbol{H}^\delta_\infty(\hat{\boldsymbol{x}}_{\boldsymbol{l}};k_{\boldsymbol{l}}) - \boldsymbol{H}_\infty(\hat{\boldsymbol{x}}_{\boldsymbol{l}};k_{\boldsymbol{l}})\right)\right| \\
&\le \frac{4\pi}{k_{\boldsymbol{l}}a^3|\hat{\boldsymbol{x}}_{\boldsymbol{l}}\times\boldsymbol{p}|}\delta\left|\boldsymbol{H}_\infty(\hat{\boldsymbol{x}}_{\boldsymbol{l}};k_{\boldsymbol{l}})\right| \\
&\le \frac{\delta}{a^3|\hat{\boldsymbol{x}}_{\boldsymbol{l}}\times\boldsymbol{p}|}\left|\hat{\boldsymbol{x}}\times\int_D e^{-\mathrm{i}k\hat{\boldsymbol{x}}_{\boldsymbol{l}}\cdot\boldsymbol{y}}\boldsymbol{J}(y)\,\mathrm{d}\boldsymbol{y}\right| \\
&\le \frac{\delta}{a^3|\hat{\boldsymbol{x}}_{\boldsymbol{l}}\times\boldsymbol{p}|}|\hat{\boldsymbol{x}}\times\boldsymbol{p}|\left|\int_D e^{-\mathrm{i}k\hat{\boldsymbol{x}}_{\boldsymbol{l}}\cdot\boldsymbol{y}}\,(f(\boldsymbol{y}) + |\nabla g(\boldsymbol{y})|)\,\mathrm{d}\boldsymbol{y}\right| \\
&\le \frac{\delta}{a^3}\left(\int_D\left|e^{-\mathrm{i}k\hat{\boldsymbol{x}}_{\boldsymbol{l}}\cdot\boldsymbol{y}}\right|^2\mathrm{d}\boldsymbol{y}\right)^{1/2}\left(\|f\|_{L^2(D)} + \|\nabla g\|_{(L^2(D))^3}\right) \\
&\le C_1\delta
\end{aligned}$$

where $C_1 = (\|f\|_{L^2(D)} + \|g\|_{H^1(D)})/a^{3/2}$ and it leads to estimate (4.1).

Correspondingly, from (3.9), we have

$$\begin{aligned}|\hat{g}_{\boldsymbol{l}}^{\delta}-\hat{g}_{\boldsymbol{l}}| &= \left|-\frac{2\hat{\boldsymbol{x}}_{\boldsymbol{l}}\times(\boldsymbol{p}\times\boldsymbol{l})}{k_{\boldsymbol{l}}a^2|\hat{\boldsymbol{x}}_{\boldsymbol{l}}\times(\boldsymbol{p}\times\boldsymbol{l})|^2}\cdot\left(\boldsymbol{H}_{\infty}^{\delta}(\hat{\boldsymbol{x}}_{\boldsymbol{l}};k_{\boldsymbol{l}})-\boldsymbol{H}_{\infty}(\hat{\boldsymbol{x}}_{\boldsymbol{l}};k_{\boldsymbol{l}})\right)\right|\\ &\le \frac{2}{k_{\boldsymbol{l}}a^2|\hat{\boldsymbol{x}}_{\boldsymbol{l}}\times(\boldsymbol{p}\times\boldsymbol{l})|}\delta\left|\boldsymbol{H}_{\infty}(\hat{\boldsymbol{x}}_{\boldsymbol{l}};k_{\boldsymbol{l}})\right|\\ &\le \frac{\delta}{2\pi|\boldsymbol{l}|a^2|\hat{\boldsymbol{x}}_{\boldsymbol{l}}\times\boldsymbol{p}|}\left|\hat{\boldsymbol{x}}\times\int_D e^{-\mathrm{i}k\hat{\boldsymbol{x}}_{\boldsymbol{l}}\cdot\boldsymbol{y}}\boldsymbol{J}(y)\,\mathrm{d}\boldsymbol{y}\right|\\ &\le \frac{\|f\|_{L^2(D)}+\|g\|_{H^1(D)}}{2\pi|\boldsymbol{l}|a^{1/2}}\ \delta\\ &\le C_2\delta,\end{aligned}$$

where $C_2=(\|f\|_{L^2(D)}+\|g\|_{H^1(D)})/(2\pi a^{1/2})$ and it verifies (4.2).

For $\boldsymbol{l}=\{\boldsymbol{0}\}$, from Schwarz inequality and (3.16), we have

$$\begin{aligned}|\hat{f}_{\boldsymbol{0}}^{\delta}-\hat{f}_{\boldsymbol{0}}| \le& \frac{\lambda\pi}{a^3\sin\lambda\pi}\left|\frac{4\pi\hat{\boldsymbol{x}}_{\boldsymbol{0}}\times\boldsymbol{p}}{\mathrm{i}k_{\boldsymbol{0}}|\hat{\boldsymbol{x}}_{\boldsymbol{0}}\times\boldsymbol{p}|^2}\cdot\left(\boldsymbol{H}_{\infty}^{\delta}(\hat{\boldsymbol{x}}_{\boldsymbol{0}};k_{\boldsymbol{0}})-\boldsymbol{H}_{\infty}(\hat{\boldsymbol{x}}_{\boldsymbol{0}};k_{\boldsymbol{0}})\right)\right|\\ &+\underbrace{\frac{\lambda\pi}{a^3\sin\lambda\pi}\sum_{1\le|\boldsymbol{l}|_{\infty}\le N}\left|\left(\hat{f}_{\boldsymbol{l}}^{\delta}-\hat{f}_{\boldsymbol{l}}\right)\int_D \mathrm{e}^{\mathrm{i}(k_{\boldsymbol{l}}\hat{\boldsymbol{l}}-k_{\boldsymbol{0}}\hat{\boldsymbol{x}}_{\boldsymbol{0}})\cdot\boldsymbol{y}}\,\mathrm{d}\boldsymbol{y}\right|}_{I_1}\\ &+\underbrace{\frac{\lambda\pi}{a^3\sin\lambda\pi}\sum_{|\boldsymbol{l}|_{\infty}\ge N}\left|\hat{f}_{\boldsymbol{l}}\int_D \mathrm{e}^{\mathrm{i}(k_{\boldsymbol{l}}\hat{\boldsymbol{l}}-k_{\boldsymbol{0}}\hat{\boldsymbol{x}}_{\boldsymbol{0}})\cdot\boldsymbol{y}}\,\mathrm{d}\boldsymbol{y}\right|}_{I_2}\\ \triangleq& C_3\delta+I_1+I_2.\end{aligned}$$

where $C_3=\lambda\pi(\|f\|_{L^2(D)}+\|g\|_{H^1(D)})/(a^{9/2}\sin\lambda\pi)$.

Define $\boldsymbol{l}=(l_1,l_2,l_3)\in\mathbb{Z}^3$, from (3.5) and (3.6), we find that

$$\int_D \mathrm{e}^{\mathrm{i}(k_{\boldsymbol{l}}\hat{\boldsymbol{l}}-k_{\boldsymbol{0}}\hat{\boldsymbol{x}}_{\boldsymbol{0}})\cdot\boldsymbol{y}}\,\mathrm{d}\boldsymbol{y}=\begin{cases}\dfrac{a^3\sin(l_1-\lambda)\pi}{(l_1-\lambda)\pi}, & |\boldsymbol{l}|=|l_1|,\\ 0, & |\boldsymbol{l}|\ne|l_1|,\end{cases}$$

which together with (4.1) gives

$$\begin{aligned}I_1 \le& \frac{\lambda\pi}{a^3\sin\lambda\pi}\sum_{1\le|\boldsymbol{l}|_{\infty}\le N}\left|\hat{f}_{\boldsymbol{l}}^{\delta}-\hat{f}_{\boldsymbol{l}}\right|\left|\frac{a^3\sin(l_1-\lambda)\pi}{(l_1-\lambda)\pi}\right|\\ \le& \frac{\lambda\pi}{\sin\lambda\pi}2\sum_{j=1}^{N}\left(C_1\delta\frac{\sin\lambda\pi}{(j-\lambda)\pi}\right)\\ \le& C_4\lambda N\delta,\end{aligned}$$

where $C_4=2C_1$. On the other hand, one can deduce that

$$\begin{aligned}I_2 \le& \frac{\lambda\pi}{a^3\sin\lambda\pi}\sum_{|\boldsymbol{l}|_{\infty}>N}|\hat{f}_{\boldsymbol{l}}|\left|\frac{a^3\sin(l_1-\lambda)\pi}{(l_1-\lambda)\pi}\right|\\ \le& \frac{\lambda\pi}{\sin\lambda\pi}\left(\sum_{|\boldsymbol{l}|_{\infty}>N}|\hat{f}_{\boldsymbol{l}}|^2\right)^{1/2}\left(\sum_{|\boldsymbol{l}|_{\infty}>N}\left|\frac{\sin(l_1-\lambda)\pi}{(l_1-\lambda)\pi}\right|^2\right)^{1/2}\\ \le& \frac{\lambda\pi}{\sin\lambda\pi}\frac{1}{a^3}\|f\|_{L^2(D)}\left(2\sum_{j=N+1}^{\infty}\left|\frac{\sin\lambda\pi}{(j-\lambda)\pi}\right|^2\right)^{1/2}\\ \le& \frac{2\lambda}{a^3\sqrt{N}}\|f\|_{L^2(D)}\\ =& C_5\frac{\lambda}{\sqrt{N}},\end{aligned}$$

where $C_5 = 2\|f\|_{L^2(D)}/a^3$. Finally, we obtain

$$|\hat{f}_{\mathbf{0}}^{\delta} - \hat{f}_{\mathbf{0}}| \le C_3\delta + C_4\lambda N\delta + C_5\frac{\lambda}{\sqrt{N}}.$$

The proof is complete. □

Lemma 4.1 ([19]). *Let $\boldsymbol{J}$ be a vector function in $(H_{\boldsymbol{p}}^{\sigma}(D))^3$ and $0 \le \mu \le \sigma$, then the following estimate holds*

$$\|\boldsymbol{J}_N - \boldsymbol{J}\|_{\boldsymbol{p},\mu} \le N^{\mu-\sigma}\|\boldsymbol{J}\|_{\boldsymbol{p},\sigma}, \quad 0 \le \mu \le \sigma.$$

The stability result is contained in the following theorem.

Theorem 4.2. *Let $\boldsymbol{J} \in (H_{\boldsymbol{p}}^{\sigma}(D))^3$ and $0 \le \mu \le \sigma$, then the following estimate holds*

$$\|\boldsymbol{J}_N^{\delta} - \boldsymbol{J}\|_{\boldsymbol{p},\mu} \le C_6\delta + C_6\lambda N\delta + C_6\frac{\lambda}{\sqrt{N}} + C_7N^{\mu+3/2}\delta + C_8N^{\mu+5/2}\delta + N^{\mu-\sigma}\|\boldsymbol{J}\|_{\boldsymbol{p},\sigma},$$

where C_6, C_7, C_8 depend only on f, g, a and λ.

Proof. It is readily seen that

$$\begin{aligned}
&\|\boldsymbol{J}_N^{\delta} - \boldsymbol{J}_N\|_{\boldsymbol{p},\mu}\\
\le&\left(\sum_{|\boldsymbol{l}|_\infty=0}^{N}\left(1+|\boldsymbol{l}|^2\right)^{\mu}|\hat{f}_{\boldsymbol{l}}^{\delta} - \hat{f}_{\boldsymbol{l}}|^2 + \frac{4\pi^2}{a^2}\sum_{|\boldsymbol{l}|_\infty=1}^{N}\left(1+|\boldsymbol{l}|^2\right)^{\mu}|\boldsymbol{p}\times\boldsymbol{l}|^2|\hat{g}_{\boldsymbol{l}}^{\delta} - \hat{g}_{\boldsymbol{l}}|^2\right)^{1/2}\\
\le&|\hat{f}_{\mathbf{0}}^{\delta} - \hat{f}_{\mathbf{0}}| + \left(\sum_{|\boldsymbol{l}|_\infty=1}^{N}\left(1+|\boldsymbol{l}|^2\right)^{\mu}|\hat{f}_{\boldsymbol{l}}^{\delta} - \hat{f}_{\boldsymbol{l}}|^2\right)^{1/2}\\
&+\left(\frac{4\pi^2}{a^2}\sum_{|\boldsymbol{l}|_\infty=1}^{N}\left(1+|\boldsymbol{l}|^2\right)^{\mu}|\boldsymbol{p}\times\boldsymbol{l}|^2|\hat{g}_{\boldsymbol{l}}^{\delta} - \hat{g}_{\boldsymbol{l}}|^2\right)^{1/2}\\
\le&\left(C_3\delta + C_4\lambda N\delta + C_5\frac{\lambda}{\sqrt{N}}\right) + C_1\delta\left(\sum_{|\boldsymbol{l}|_\infty=1}^{N}\left(1+|\boldsymbol{l}|^2\right)^{\mu}\right)^{1/2}\\
&+\frac{2\pi}{a}C_2\delta\left(\sum_{|\boldsymbol{l}|_\infty=1}^{N}\left(1+|\boldsymbol{l}|^2\right)^{\mu}|\boldsymbol{l}|^2\right)^{1/2}\\
\le&C_6\delta + C_6\lambda N\delta + C_6\frac{\lambda}{\sqrt{N}} + C_7N^{\mu+3/2}\delta + C_8N^{\mu+5/2}\delta,
\end{aligned} \tag{4.4}$$

where $C_6 = \max\{C_3, C_4, C_5\}$. Hence, from (4.4) and Lemma 4.1, we obtain

$$\|\boldsymbol{J}_N^{\delta} - \boldsymbol{J}\|_{\boldsymbol{p},\mu} \le C_6\delta + C_6\lambda N\delta + C_6\frac{\lambda}{\sqrt{N}} + C_7N^{\mu+3/2}\delta + C_8N^{\mu+5/2}\delta + N^{\mu-\sigma}\|\boldsymbol{J}\|_{\boldsymbol{p},\sigma},$$

which completes the proof. □

Remark 4.1. If one takes $N = \tau\delta^{-\frac{1}{\sigma+5/2}}$ with $\tau \ge 1$ in Theorem 4.2 , we have

$$\begin{aligned}
\|\boldsymbol{J}_N^{\delta} - \boldsymbol{J}\|_{\boldsymbol{p},\mu} \le& C_6\delta + C_6\lambda\tau\delta^{\frac{\sigma+3/2}{\sigma+5/2}} + \frac{C_6\lambda}{\sqrt{\tau}}\delta^{\frac{1}{2\sigma+5}} + C_7\tau^{\mu+3/2}\delta^{\frac{1+\sigma-\mu}{\sigma+5/2}}\\
&+ C_8\tau^{\mu+5/2}\delta^{\frac{\sigma-\mu}{\sigma+5/2}} + \tau^{\mu-\sigma}\delta^{\frac{\sigma-\mu}{\sigma+5/2}}\|\boldsymbol{J}\|_{\boldsymbol{p},\sigma}, \quad 0 \le \mu \le \sigma.
\end{aligned}$$

Remark 4.2. Since only a finite number of wavenumbers are available in reality, the reconstruction of $\boldsymbol{J}$ should be understood as finding an approximation $\boldsymbol{J}_N$. Moreover, it can be seen from Theorem 4.2 that the truncation N plays the role of regularization in some sense. However, the optimal choice of this truncation N is complicated and currently open. In this regard, we would like to point out that, although we have established the uniqueness in Theorem 3.1 and stability in Theorem 4.2, the original inverse source problem is still ill-posed.

5. Numerical examples

In this section, we carry out a series of numerical experiments to illustrate that the proposed Fourier reconstruction method is effective and efficient.

First, we briefly describe some parameter settings of our numerical experiments. Let $D = [-0.5, 0.5]^3$, namely, $a = 1$. Assume that the wave propagates in the vacuum space, where $\mu_0 = 4\pi \times 10^{-7}$ and $\varepsilon_0 = 8.8541 \times 10^{-12}$. Synthetic electromagnetic far-field data are generated by solving the direct problem of (2.1) by using the quadratic finite elements on a truncated spherical domain enclosed by a PML layer. The mesh of the forward solver is successively refined till the relative error of the successive measured electromagnetic wave data is below 0.1%. To show the stability of our proposed method, we also add some random noise to the synthetic far-field data by considering

$$\boldsymbol{E}_\infty^\delta := \left(E_{\infty,1}^\delta,\ E_{\infty,2}^\delta,\ E_{\infty,3}^\delta\right)^\top, \quad \boldsymbol{H}_\infty^\delta := \left(H_{\infty,1}^\delta,\ H_{\infty,2}^\delta,\ H_{\infty,3}^\delta\right)^\top,$$

where

$$E_{\infty,i}^\delta = E_{\infty,i} + \delta r_1 |E_{\infty,i}| e^{i\pi r_2}, \quad H_\infty^\delta = H_{\infty,i} + \delta r_1 |H_{\infty,i}| e^{i\pi r_2}, \quad i = 1, 2, 3,$$

r_1 and r_2 are two uniform random numbers, both ranging from -1 to 1, and $\delta > 0$ represents the noise level. From Remark 4.1, the truncation N is given by

$$N(\delta) := [3\delta^{-2/7}] + 1, \tag{5.1}$$

where $[X]$ denotes the largest integer that is smaller than $X + 1$.

Next, we specify details of obtaining the artificial multi-frequency electromagnetic far-field data. Let

$$\mathbb{L}_N := \{\boldsymbol{l} \in \mathbb{Z}^3 \mid 1 \le |\boldsymbol{l}|_\infty \le N\},$$

then the wavenumber set is given by

$$\mathbb{K}_N := \{2\pi|\boldsymbol{l}| : \boldsymbol{l} \in \mathbb{L}_N\} \cup \{2\pi\lambda\}, \quad \lambda = 10^{-3},$$

and the observation directions are given by

$$\mathbb{X}_N := \left\{\frac{\boldsymbol{l}}{|\boldsymbol{l}|} : \boldsymbol{l} \in \mathbb{L}_N\right\} \cup \{(1, 0, 0)\}.$$

Thus, every wavenumber and observation direction can be denoted by $k_j \in \mathbb{K}_N$ and $\hat{\boldsymbol{x}}_j \in \mathbb{X}_N$, respectively, where $j = 1, 2, \ldots, (2N+1)^3$. Correspondingly, the frequency ω_j is chosen as $\omega_j = k_j/\sqrt{\mu_0\varepsilon_0}$. With the admissible wavenumbers defined earlier, the artificial electromagnetic far-field data with noise can be written as

$$\left\{\left(\boldsymbol{E}_\infty^\delta(\hat{x}_j; k_j, \boldsymbol{p}), \boldsymbol{H}_\infty^\delta(\hat{x}_j; k_j, \boldsymbol{p})\right) : \hat{\boldsymbol{x}}_j \in \mathbb{X}_N, k_j \in \mathbb{K}_N,\ j = 1, 2, \ldots, (2N+1)^3\right\},$$

where $\boldsymbol{p}$ is a given polarization direction and it satisfies

$$\mathbb{P}_N := \left\{\boldsymbol{p} \in \mathbb{S}^2 \mid \boldsymbol{p} \times \boldsymbol{l} \ne \boldsymbol{0}, \quad \forall\, \boldsymbol{l} \in \mathbb{L}_N\right\}. \tag{5.2}$$

Finally, we specify details of the numerical inversion via the Fourier method. We reconstruct the electric current source $\boldsymbol{J}(\boldsymbol{x})$, $\boldsymbol{x} \in D$ by the truncated Fourier expansion $\boldsymbol{J}_N^\delta(\boldsymbol{x})$, $\boldsymbol{x} \in D$, where

$$\boldsymbol{J} = (J_1,\ J_2,\ J_3)^\top, \quad \boldsymbol{J}_N^\delta = \left(J_{1,N},\ J_{2,N},\ J_{3,N}\right)^\top.$$

Given the noisy far-field data defined above, if we use the electric far-field data $\{\boldsymbol{E}_\infty^\delta(\hat{\boldsymbol{x}}_j; k_j, \boldsymbol{p})\}$, then the Fourier coefficients $\hat{f}_{\boldsymbol{l}}, \hat{g}_{\boldsymbol{l}}$, $1 \le |\boldsymbol{l}|_\infty \le N$ and $\hat{f}_{\boldsymbol{0}}$ are computed by (3.13), (3.14) and (3.17), respectively. If we use the magnetic far-field data $\{\boldsymbol{H}_\infty^\delta(\hat{\boldsymbol{x}}_j; k_j, \boldsymbol{p})\}$, then the Fourier coefficients $\hat{f}_{\boldsymbol{l}}, \hat{g}_{\boldsymbol{l}}$, $1 \le |\boldsymbol{l}|_\infty \le N$ and $\hat{f}_{\boldsymbol{0}}$ are computed by (3.8), (3.9) and (3.16), respectively. Divide the domain D into a mesh with a uniform grid of size $50 \times 50 \times 50$. The approximated Fourier series $\boldsymbol{J}_N^\delta(\boldsymbol{z})$ are computed at the mesh nodes $\boldsymbol{z}_j$, $j = 1, 2, \ldots, 50^3$ by (3.15). The relative error is defined as

$$\text{relative error} = \|\boldsymbol{J} - \boldsymbol{J}_N^\delta\|_{(L^2(D))^3} / \|\boldsymbol{J}\|_{(L^2(D))^3}.$$

Unless specified otherwise, we use the magnetic far-field data to reconstruct the electromagnetic source.

Based on the above discussion, we formulate the reconstruction scheme by the Fourier method in Algorithm S as follows.

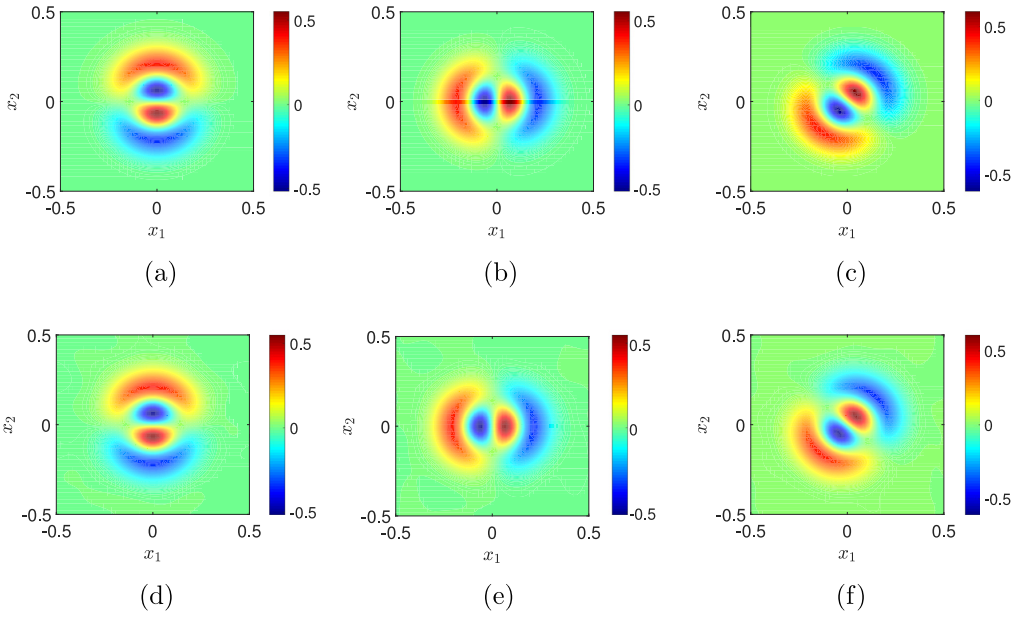

Fig. 2. Contour plots of the exact and reconstructed source function of Example 1 at the plane $x_3 = 0$, where $\delta = 2\%$. (a) J_1, (b) J_2, (c) J_3, (d) $J_{1,10}$, (e) $J_{2,10}$, (f) $J_{3,10}$.

Table 1
The relative errors of the reconstructions with different noise levels δ.

δ	2%	5%	10%	20%
$N(\delta)$	10	8	6	5
Relative error	0.10%	2.10%	4.26%	8.94%
Time (s)	78.3	40.1	11.9	10.7

Algorithm S:	Fourier method for reconstructing the electromagnetic source
Step 1	Choose the parameters λ, N, the wavenumber set $\mathbb{K}_N$ and observation direction set $\mathbb{X}_N$.
Step 2	For a given $\boldsymbol{p} \in \mathbb{P}_N$ defined in (5.2) , measure the electric far-field data $\boldsymbol{E}_\infty^\delta(\hat{\boldsymbol{x}}_j; k_j, \boldsymbol{p})$ or the magnetic far-field data $\boldsymbol{H}_\infty^\delta(\hat{\boldsymbol{x}}_j; k_j, \boldsymbol{p})$ for $\hat{\boldsymbol{x}}_j \in \mathbb{X}_N$ and $k_j \in \mathbb{K}_N$.
Step 3	Compute the Fourier coefficients $\hat{f}_{\boldsymbol{0}}$, $\hat{f}_{\boldsymbol{l}}$ and $\hat{g}_{\boldsymbol{l}}$ for $1 \le \lvert\boldsymbol{l}\rvert_\infty \le N$.
Step 4	Furthermore, select a sampling mesh $\mathcal{T}_h$ in D. For each sampling point $\boldsymbol{z}_j \in \mathcal{T}_h$, calculate the imaging functional $\boldsymbol{J}_N$ defined in (3.15), then $\boldsymbol{J}_N$ is the reconstruction of $\boldsymbol{J}$.

Remark 5.1. The codes in the following numerical experiments are written in MATLAB 2016b and run on a desktop with Intel Core i7 CPU of 3.40 GHz.

Example 1. In this example, we numerically estimate the stability of the proposed method. We consider the following smooth source function

$$\boldsymbol{J} = \boldsymbol{p} \times \nabla g,$$

where

$$\boldsymbol{p} = \frac{1}{4}\left(\sqrt{5}, -2, \sqrt{7}\right),$$
$$g(x_1, x_2, x_3) = 10\left(x_1^2 + x_2^2\right)\exp\left(-50\left(x_1^2 + x_2^2 + x_3^2\right)\right).$$

Fig. 2 shows the comparison between the exact and the reconstructed source function at the plane $x_3 = 0$ with the additional noise $\delta = 2\%$. We observe that the reconstructions are very close to the exact one. To exhibit the accuracy quantitatively, we list the relative errors in L^2 in Table 1. Meanwhile, Table 1 illustrates that the stability and CPU time increases as the truncation order $N(\delta)$ increases.

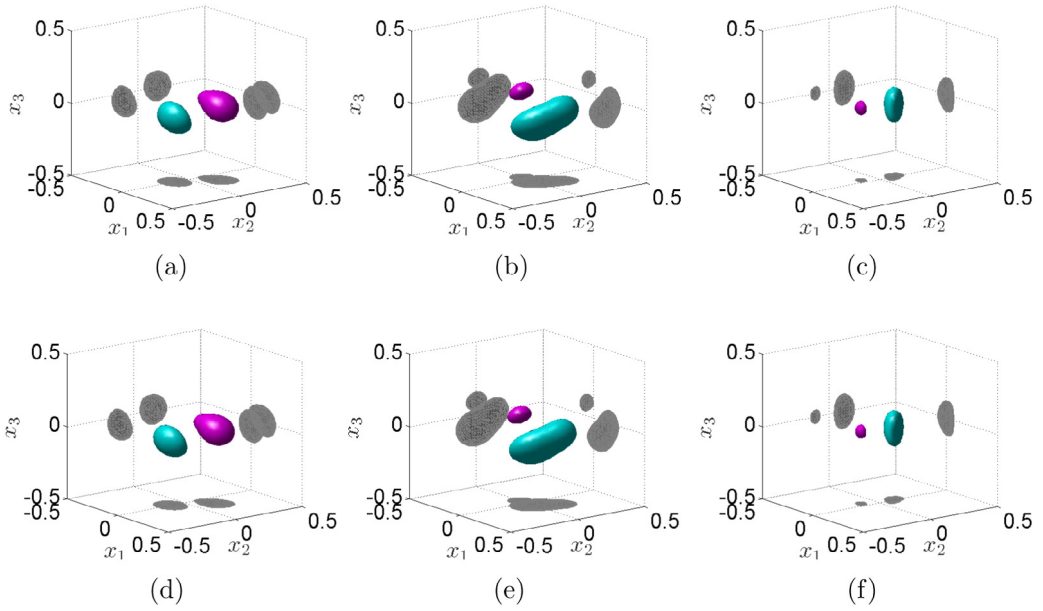

Fig. 3. Iso-surface plots of the exact and the reconstructed vectorial source function of Example 2, where the red color denotes the iso-surface level being 1.2 and the green color denotes iso-surface level being −0.6. (a) J_1, (b) J_2, (c) J_3, (d) $J_{1,10}$, (e) $J_{2,10}$, (f) $J_{3,10}$. (For interpretation of the references to color in this figure legend, the reader is referred to the web version of this article.)

Example 2. From (2.4) and (2.5), it is clear that

$$\boldsymbol{E}_\infty(-\hat{\boldsymbol{x}}) = -\overline{\boldsymbol{E}_\infty(\hat{\boldsymbol{x}})}, \quad \boldsymbol{H}_\infty(-\hat{\boldsymbol{x}}) = \overline{\boldsymbol{H}_\infty(\hat{\boldsymbol{x}})}.$$

Therefore, for our inverse problem, the measurements of the far-field data could be from an upper hemisphere $\mathbb{S}^2_+$, say $x_3 \geq 0$. In this example, we use the electric far-field data from an upper hemisphere $\mathbb{S}^2_+$ to recover the source. We aim to recover a smooth source as follows

$$\boldsymbol{J} = \boldsymbol{p}f + \boldsymbol{p} \times \nabla g;$$

where

$$\boldsymbol{p} = \frac{1}{3}\left(\sqrt{5}, -1, \sqrt{3}\right),$$
$$f(x_1, x_2, x_3) = 3\exp\left(-80\left((x_1 - 0.15)^2 + (x_2 - 0.15)^2 + x_3^2\right)\right),$$
$$g(x_1, x_2, x_3) = 0.3\exp\left(-40\left(x_1^2 + x_2^2 + x_3^2\right)\right).$$

Fig. 3 presents the iso-surface plots of the exact source and the reconstruction with 2% noise , which demonstrate clearly that our proposed method performs nicely.

Example 3. In this example, we consider a discontinuous source function. For simplicity, the source function is given by

$$\boldsymbol{J} = \boldsymbol{p}f,$$

where

$$\boldsymbol{p} = \frac{1}{\sqrt{6}}\left(1, \sqrt{2}, \sqrt{3}\right),$$

$$f(x_1, x_2, x_3) = \begin{cases} 1, & \text{if } (x_1 + 0.25)^2 + x_2^2 + x_3^2 \leq 0.15^2, \\ \dfrac{1}{2}, & \text{if } 0.1 \leq x_1 \leq 0.4, -0.15 \leq x_2 \leq 0.15, -0.15 \leq x_3 \leq 0.15, \\ 0, & \text{elsewhere.} \end{cases}$$

Fig. 4 shows the contour plots of the exact source and the reconstructions with different truncation order, $N = 5, 10, 15, 20, 25$. It is clear that the resolution of the reconstructed results increases as the truncation order N increases. Fig. 5 shows the Gibbs phenomenon of the reconstructions over the line $x_2 = x_3 = 0$ with the truncation order $N = 5, 15, 25$, respectively.

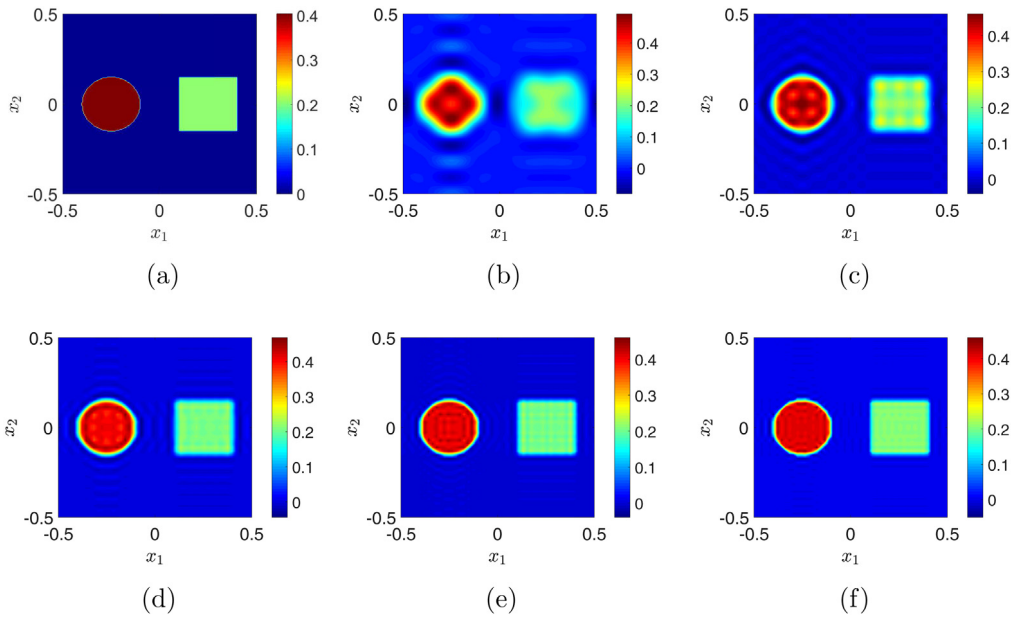

Fig. 4. Contour plots of the exact and the reconstructed vector source function in Example 3 at the plane $x_3 = 0$. (a) exact J_1, (b) $J_{1,5}$, (c) $J_{1,10}$, (d) $J_{1,15}$, (e) $J_{1,20}$, (f) $J_{1,25}$.

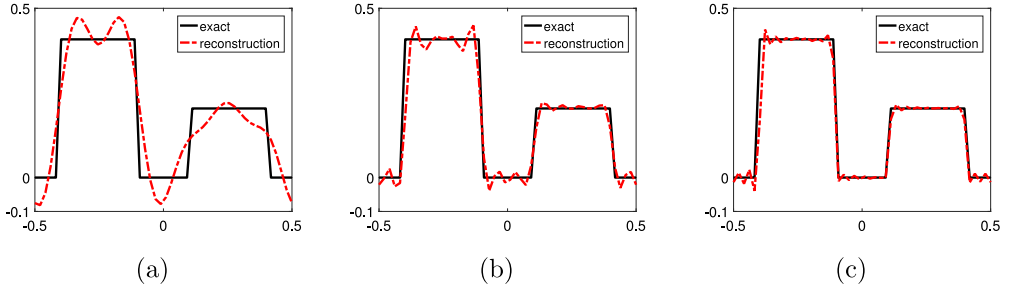

Fig. 5. Gibbs phenomenon of the reconstructed source $J_{1,N}$ for different N with $x_2 = x_3 = 0$. (a) $N = 5$, (b) $N = 15$, (c) $N = 25$.

Example 4. In the final example, we try to recover the source with partial data. For simplicity, the source function is given by

$$\boldsymbol{J} = \boldsymbol{p}f,$$

where

$$\begin{aligned}
\boldsymbol{p} &= \frac{1}{\sqrt{6}}\left(1, \sqrt{2}, \sqrt{3}\right),\\
f(x_1, x_2, x_3) &= \exp\left(-200\left((x_1 + 0.15)^2 + (x_2 + 0.15)^2 + x_3^2\right)\right)\\
&\quad + \exp\left(-200\left((x_1 + 0.15)^2 + (x_2 - 0.15)^2 + x_3^2\right)\right)\\
&\quad + \exp\left(-200\left((x_1 - 0.15)^2 + (x_2 + 0.15)^2 + x_3^2\right)\right)\\
&\quad + \exp\left(-200\left((x_1 - 0.15)^2 + (x_2 - 0.15)^2 + x_3^2\right)\right).
\end{aligned}$$

Let θ and φ denote, respectively, the polar and azimuthal angle in the spherical coordinates. By the symmetry, the measurements of far-field data could be collected from an upper hemisphere $\mathbb{S}^2_+$, that is $x_3 \geq 0$. Then we could obtain $\theta \in [0, \pi/2]$ and $\varphi \in [-\pi, \pi]$. Fig. 6 shows the reconstructions of $\boldsymbol{J}_1$ with partial measured data, where the truncation order is $N = 15$. It is clear that the quality of reconstructions deteriorates as the observation angles shrink. Thus it is reasonable to expect that the reconstruction would be barely detectable if the measured data is from only a very limited aperture. In particular, Fig. 6(i) shows that the reconstructed source is almost invisible when $\theta = [0, \pi/6]$, $\varphi = [-\pi/3, \pi/3]$.

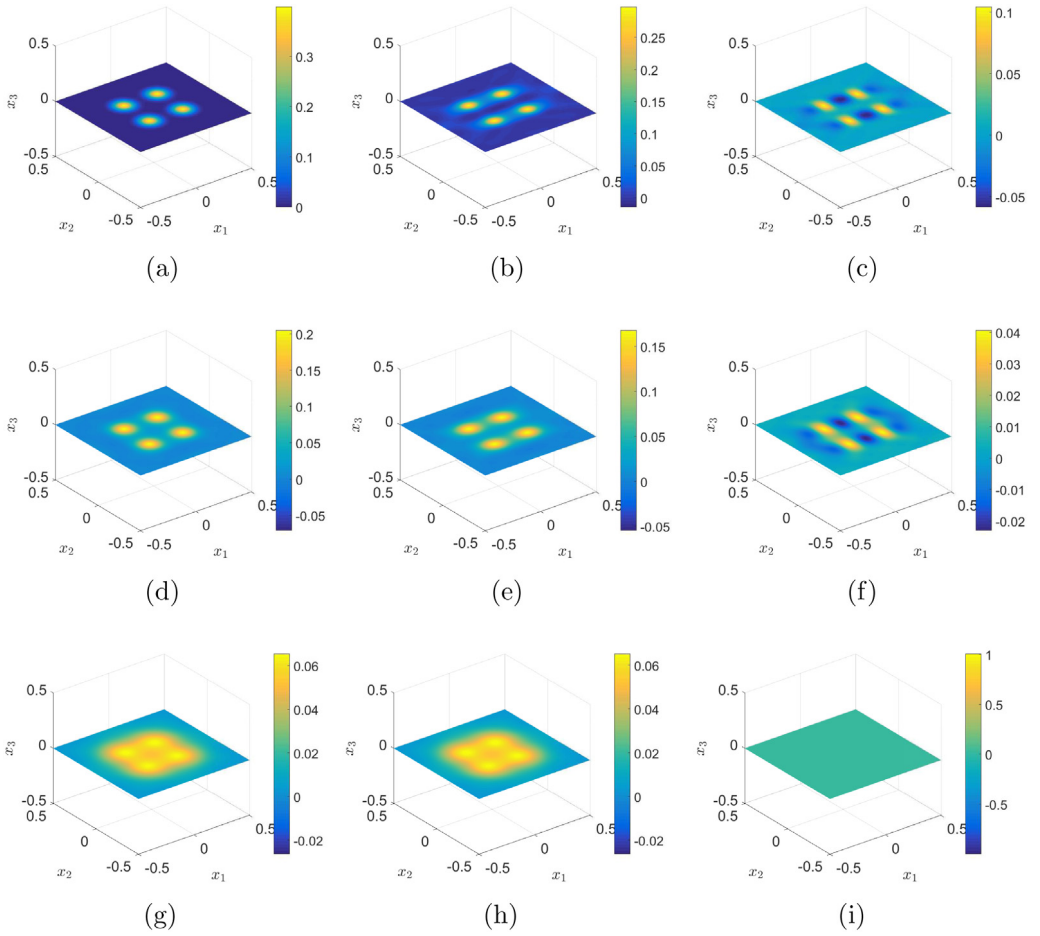

Fig. 6. Reconstruction of source $J_{1,15}$ with 10% noise. (a) $\theta = [0, \pi/2]$, $\varphi = [-\pi, \pi]$, (b) $\theta = [0, \pi/2]$, $\varphi = [-2\pi/3, 2\pi/3]$, (c) $\theta = [0, \pi/2]$, $\varphi = [-\pi/3, \pi/3]$, (d) $\theta = [0, \pi/3]$, $\varphi = [-\pi, \pi]$, (e) $\theta = [0, \pi/3]$, $\varphi = [-2\pi/3, 2\pi/3]$, (f) $\theta = [0, \pi/3]$, $\varphi = [-\pi/3, \pi/3]$, (g) $\theta = [0, \pi/6]$, $\varphi = [-\pi, \pi]$, (h) $\theta = [0, \pi/6]$, $\varphi = [-2\pi/3, 2\pi/3]$, (i) $\theta = [0, \pi/6]$, $\varphi = [-\pi/3, \pi/3]$.

Acknowledgments

The work of M. Song was supported by the NSF, China grant of China under 11671113. The work of Y. Guo was supported by the NSF, China grants of China under 11601107, 11671111 and 41474102. The work of H. Liu was supported by the FRG, China and startup grants from Hong Kong Baptist University, Hong Kong RGC General Research Funds, 12302415 and 12302017. The authors would also like to thank the anonymous referees for their insightful and constructive comments and suggestions on this work.

References

[1] M. Anastasio, J. Zhang, D. Modgil, P. La Rivi, Application of inverse source concepts to photoacoustic tomography, Inverse Problems 23 (6) (2007) 21–35.
[2] C. Clason, M. Klibanov, The quasi-reversibility method for thermoacoustic tomography in a heterogeneous medium, SIAM J. Sci. Comput. 30 (1) (2007) 1–23.
[3] M. Klibanov, Thermoacoustic tomography with an arbitrary elliptic operator, Inverse Problems 29 (2) (2013) 025014.
[4] H. Liu, G. Uhlmann, Determining both sound speed and internal source in thermo- and photo-acoustic tomography, Inverse Problems 31 (10) (2015) 105005.
[5] H. Ammari, G. Bao, J. Fleming, An inverse source problem for Maxwell's equations in magnetoencephalography, SIAM J. Appl. Math. 62 (4) (2002) 1369–1382.
[6] S. Arridge, Optical tomography in medical imaging, Inverse Problems 15 (2) (1999) R41–R93.
[7] A. Fokas, Y. Kurylev, V. Marinakis, The unique determination of neuronal currents in the brain via magnetoencephalography, Inverse Problems 20 (4) (2004) 1067–1082.
[8] A. El Badia, T. Ha-Duong, On an inverse source problem for the heat equation. Application to a pollution detection problem, J. Inverse Ill-Posed Probl. 10 (6) (2002) 585–599.

[9] G. Bao, P. Li, Y. Zhao, Stability in the inverse source problem for elastic and electromagnetic waves with multi-frequencies, 2017, arXiv:1703.03890v1.
[10] V. Isakov, Inverse Source Problems, Mathematical Surveys and Monographs, American Mathematical Society, Providence, 1990.
[11] A. Alzaalig, G. Hu, X. Liu, J. Sun, Fast acoustic source imaging using multi-frequency sparse data, 2017, arXiv:1712.02654.
[12] A. El Badia, T. Nara, Inverse dipole source problem for time-harmonic Maxwell equations: algebraic algorithm and Hölder stability, Inverse Problems 29 (1) (2013) 015007.
[13] S. He, V. Romanov, Identification of dipole sources in a bounded domain for Maxwell's equations, Wave Motion 28 (1) (1998) 25–40.
[14] M. Eller, N. Valdivia, Acoustic source identification using multiple frequency information, Inverse Problems 25 (11) (2009) 115005.
[15] N. Valdivia, Electromagnetic source identification using multiple frequency information, Inverse Problems 28 (11) (2012) 115002.
[16] N. Bleistein, J. Cohen, Nonuniqueness in the inverse source problem in acoustics and electromagnetics, J. Math. Phys. 18 (2) (1977) 194–201.
[17] E. Marengo, A. Devaney, Nonradiating sources with connections to the adjoint problem, Phys. Rev. E. 70 (2004) 037601.
[18] R. Albanese, P. Monk, The inverse source problem for Maxwell's equations, Inverse Problems 22 (3) (2006) 1023–1035.
[19] G. Wang, F. Ma, Y. Guo, J. Li, Solving the multi-frequency electromagnetic inverse source problem by the Fourier method, J. Differential Equations 265 (1) (2018) 417–443.
[20] X. Wang, Y. Guo, D. Zhang, H. Liu, Fourier method for recovering acoustic sources from multi-frequency far-field data, Inverse Problems 33 (3) (2017) 035001.
[21] D. Zhang, Y. Guo, Fourier method for solving the multi-frequency inverse source problem for the Helmholtz equation, Inverse Problems 31 (3) (2015) 035007.
[22] C. Tai, Dyadic Green Functions in Electromagnetic Theory, IEEE, New York, 1994, pp. 48–50.
[23] D. Colton, R. Kress, Inverse Acoustic and Electromagnetic Scattering Theory, third ed., Springer-Verlag, Berlin, 2013.
[24] I.V. Lindell, TE/TM decomposition of electromagnetic sources, IEEE Trans. Antennas and Propagation 36 (10) (1988) 1382–1388.